

**₁ Interannual to decadal changes in the western South
₂ Atlantic's surface circulation**

Rick Lumpkin and Silvia Garzoli

Rick Lumpkin, NOAA/Atlantic Oceanographic and Meteorological Laboratory, 4301 Ricken-
backer Cswy, Miami, FL USA. (Rick.Lumpkin@noaa.gov)

¹NOAA/Atlantic Oceanographic and
Meteorological Laboratory, Miami, FL USA

3 **Abstract.** A combination of surface drifters and altimetry is used to an-
4 alyze the seasonal to interannual variability of the surface velocity field in
5 the Brazil/Malvinas confluence of the western South Atlantic Ocean. Longer-
6 term changes are inferred from wind and sea surface temperature fields. Dur-
7 ing the period October 1992-December 2007, a southward shift of -0.6 to -
8 0.9 degrees per decade is found in the confluence latitude of the Brazil and
9 Malvinas currents. A comparable trend is found in the latitude of the max-
10 imum wind stress curl averaged across the South Atlantic basin, allowing a
11 proxy for the confluence latitude to be calculated for the pre-altimeter time
12 period. This longer time series suggests that the recent trend may be part
13 of a longer-term oscillation, which has returned to values last sustained in
14 the early 1980s. This variation does not appear to be related to the multi-
15 decadal trend in the Southern Annular Mode, but instead is inversely related
16 to long-term variations in sea surface temperature anomaly in the Agulhas-
17 Benguela pathway of the eastern South Atlantic subtropical basin.

1. Introduction

18 The South Atlantic's circulation presents several unique characteristics of significance
19 for climate variability. This region is the main source of equatorial surface and thermocline
20 waters [*Blanke et al.*, 1999; *Matano et al.*, 1993; *Speich et al.*, 2007], where the circulation,
21 and therefore its variability, impacts the climate of the surrounding continents by affecting
22 sea surface temperature (SST) distribution through lateral advection and/or propagating
23 anomalies within the mixed layer [*Kushnir et al.*, 2002]. The South Atlantic is open to
24 the Indian and Pacific Oceans, providing the gateway by which the Atlantic meridional
25 overturning circulation communicates with the global ocean.

26 The South Atlantic thermocline and subantarctic inflow is derived from the eastward
27 flowing South Atlantic Current [*Stramma and England*, 1999], part of which turns north-
28 ward into the Benguela Current. The Benguela Current is the broad northward flow
29 adjacent to southwestern Africa that forms the eastern limb of the South Atlantic sub-
30 tropical gyre and the origin of the upper layer water flowing northward across the equator
31 into the North Atlantic. At 30°S, the entire current is confined between the African coast
32 and the Walvis Ridge near the Greenwich meridian. Observations have revealed that at
33 30°S, the Benguela Current northward transport consists of a steady flow confined be-
34 tween the southern African coast and approximately 4°E, amounting to 10 Sv in the mean
35 (1 Sv=10⁶ m³ s⁻¹), and a transient flow (3 Sv in the mean) between 4°E and the Walvis
36 Ridge [*Garzoli and Gordon*, 1996]. The total westward transport in the Benguela Current
37 Extension above 1000 m, north of the Walvis Ridge and between 18°S-33°S is estimated
38 to be 29 Sv [*Garzoli et al.*, 1996; *Richardson and Garzoli*, 2003].

39 The Brazil and Malvinas western boundary currents dominate the western South At-
40 lantic circulation. The Brazil Current is one of the weakest western boundary currents in
41 the world, with maximum poleward transports not exceeding 30 Sv mostly confined to the
42 upper 1000 m [*Signorini*, 1978; *Gordon and Greengrove*, 1986; *Peterson and Stramma*,
43 1991; *Garzoli*, 1993]. *Stommel* [1958] first suggested that this is due to what today is
44 known as the Meridional Overturning Circulation, which requires a net northward upper
45 ocean transport across the South Atlantic to balance the southward export of North At-
46 lantic Deep Water. The Malvinas Current, a branch of the Circumpolar Current, flows
47 north along the eastern boundary of the continental shelf of Argentina. At approximately
48 38°S, the warm salty southward-flowing Brazil Current encounters the cold, fresher north-
49 ward flow of the Malvinas Current, generating a strong thermohaline front known as the
50 Confluence Front (hereafter “the confluence”) with lateral temperature gradients as high
51 as 1°C/100 m [*Gordon and Greengrove*, 1986]. After the confluence, both the Brazil and
52 Malvinas currents turn eastward and flow offshore in a series of large-scale meanders [*Gor-*
53 *don and Greengrove*, 1986] and the single Brazil/Malvinas front separates into the Brazil
54 Current Front and Subantarctic Front [*Saraceno et al.*, 2004].

55 A marked seasonal variability in the location of the confluence, up to 900 km along the
56 continental shelf break, has been observed from satellite observations [*Olson et al.*, 1988;
57 *Goni and Wainer*, 2001; *Saraceno et al.*, 2004], surface observations [*Olson et al.*, 1988],
58 and subsurface observations [*Garzoli and Bianchi*, 1987; *Garzoli and Garraffo*, 1989].
59 During austral summer (January, February, March) the confluence reaches its southern-
60 most extent; during austral winter (June, July, August) it reaches its northernmost extent.
61 Numerical studies [*Matano et al.*, 1993] indicate that this seasonal migration is governed

62 by the curl of the wind stress, which has maximum values following a similar annual cy-
63 cle. The same model also indicates that the location of the confluence depends on the
64 mass transport of the confluent currents. However, satellite altimetry [*Vivier et al.*, 2001]
65 suggests that Malvinas Current transport variations are not driving the annual variability
66 of the confluence location.

67 In addition to the seasonal variability, the latitude of separation of the Brazil cur-
68 rent from the coast has strong interannual variability that is forced by anomalous wind
69 patterns south of the confluence [*Garzoli and Giulivi*, 1994]. There is no apparent corre-
70 lation between wind-forced pulses in the Antarctic Circumpolar Current and the observed
71 anomalous northward penetration of the Malvinas Current. *Witter and Gordon* [1999]
72 concluded that interannual variations in the strength of the South Atlantic subtropical
73 gyre, and thus of the western boundary Brazil current, were driven by changes in the
74 basin-wide wind stress curl, with a strong gyre in 1993-1995 and a weak gyre in 1996-
75 1997.

76 At longer time scales, few studies have characterized the variability of the confluence.
77 SST observations from 1854-1994 in the well-observed region north of the mean frontal
78 position [*Zavialov et al.*, 1999] indicate a long-term secular warming of 1.2-1.6°C on the
79 continental shelf break, mostly since the 1940s, with interannual to decadal variance of
80 up to 2.3°C². Using the 17°C isotherm as a marker of the confluence front, *Zavialov et al.*
81 [1999] concluded that the northernmost (winter) confluence location exhibited significant
82 variability at 18, 24 and ~50 years, with a generally southward drift from its northernmost
83 location, 27.0°S in 1911, to its southernmost, 34.3°S in 1993. *Zavialov et al.* [1999] did
84 not address what has happened to the confluence since 1993, nor whether changes in the

85 northernmost winter location are also representative of the mean position of the confluence
86 front.

87 In this study, a combination of surface drifters and altimeter data will be used to analyze
88 the seasonal to interannual variability of the surface velocity field at the confluence of the
89 Brazil and Malvinas currents. We find that the confluence has shifted southward over
90 the 16-year period of TOPEX/Jason altimetry, with much of the shift concentrated in
91 the first ten years. This shift is reflected in the location of the basin-averaged wind stress
92 curl maximum, consistent with fluctuations at the seasonal time scale, suggesting that the
93 wind field can be used to derive a proxy for the confluence location in the pre-altimeter
94 time period. We exploit this to examine decadal fluctuations of the confluence location
95 since 1979.

2. Data

96 Sea level anomaly (SLA) for this study was obtained from the $1/3^\circ$ gridded Ssalto/Duacs
97 delayed-time updated (up to four satellite) altimeter product of AVISO [*Le Traon et al.*,
98 1998]. This product uses data from the following altimeters for the period October 1992–
99 December 2007: TOPEX/Poseidon (hereafter “T/P”, start to October 2005), European
100 Remote-Sensing Satellite(ERS) ERS-1 (start to May 1995), ERS-2 (May 1995–June 2003),
101 Geosat Follow-On (GFO; January 2000–), JASON-1 (April 2002–), and Envisat (June
102 2003–). SLA is best estimated when multiple satellites are in orbit, and thus the accuracy
103 of this product generally increases with time through the study period.

104 Near-surface currents are derived by combining drifter velocities with wind products and
105 altimetry. The drifters are satellite-tracked, drogued at 15 m depth [*Niiler, 2001; Lumpkin
106 and Pazos, 2007*]. Ekman currents are calculated from NCEP operational winds using the

107 *Ralph and Niiler* [1999] model, with updated coefficients from *Niiler* [2001]. The Ekman
108 drift is subtracted from the total drifter velocities to derive the residual, predominantly
109 geostrophic component of the flow. These velocities are synthesized with geostrophic
110 velocity anomalies from the gridded altimetry, using the methodology of [*Niiler et al.*,
111 2003]. This approach uses concurrent altimetric velocity anomalies and drifter velocities
112 to determine two spatially-varying parameters: a gain coefficient which must be multiplied
113 with the altimeter anomalies to match the in-situ drifter eddy kinetic energy, and the time-
114 mean unbiased current which can be added to the gain-adjusted altimetric anomalies. At
115 every spatial point, these two parameters are calculated as a temporal average over all
116 available drifter data. As a consequence, the methodology cannot produce temporally-
117 varying error estimates, although the density of altimeters and of drifters varies with time.
118 However, the strength of this approach is that it combines multiple sources of information
119 on geostrophic surface currents. This synthesis produces weekly snapshots of geostrophic
120 near-surface currents at $1/3^\circ$ resolution.

121 In order to provide an error estimate for the location of the confluence, an alternative
122 approach is used that relies solely upon altimetry. AVISO SLA and their formal error
123 estimates (also provided by AVISO) are extracted along an ascending segment of T/P
124 ground track 163, which approximately aligns with the South American continental shelf
125 break in the region of the Brazil/Malvinas Confluence (Fig. 1, top). This ground track
126 was covered by T/P from the beginning of the mission, 14 October 1992, until 15 Septem-
127 ber 2002. JASON-1 occupied this ground pass from launch in December 2001 through
128 the latest data analyzed here (December 2007). Total sea level along this track was esti-
129 mated by combining the SLA with CNES-CLS09 Mean Dynamic Topography v1.1 [*Rio*

130 *et al.*, 2009]. Estimates of the confluence location from these data are not independent of
131 estimates from the velocity product, as that uses the full gridded AVISO product which
132 includes T/P and Jason SLA. However, as described below the error estimate from sea
133 height anomaly can be propagated to an error in the confluence location, and thus this
134 approach is complementary to the approach using a synthesis of drifters, altimetry and
135 winds.

136 To analyze the behavior of the confluence for the period 1979-2007, winds, surface air
137 pressure and SST were obtained from the NCEP/NCAR v.2 Reanalysis product [*Kalnay*
138 *et al.*, 1996] (hereafter NNR). This product contains significant biases at high latitudes
139 of the Southern Hemisphere prior to the assimilation of satellite sounder data in 1979
140 [*Thompson and Solomon*, 2002], and thus we did not examine this product for earlier
141 years for this region.

3. Mean Circulation

142 The mean surface geostrophic circulation of the South Atlantic derived from the syn-
143 thesis of surface drifter trajectories, NNR winds and AVISO sea level anomalies are shown
144 in Fig. 2. This represents a mean for the altimeter time period 14 October 1992 through
145 the most recent data considered here, 31 December 2007. The mean surface characteris-
146 tics of the surface circulation are well reproduced. South of Africa, the Agulhas Current
147 enters the South Atlantic and retroflects in the mean at 22°E. The Benguela Current can
148 be observed flowing parallel to the African coasts and separating in what becomes the
149 Benguela Current extension at around 20°S. This becomes the northern branch of the
150 subtropical gyre and flows northwestward as the South Equatorial Current (SEC). The
151 SEC bifurcates when it reaches the South American continent, in the mean at 16.5°S.

152 After bifurcation, the northward North Brazil Current forms the western boundary of the
153 elongated, clockwise equatorial gyre [*Lumpkin and Garzoli, 2005*] while the southward
154 Brazil Current forms the western boundary of the subtropical gyre. The cold and fresh
155 Malvinas Current is observed as a branch of the Antarctic Circumpolar Current flowing
156 north and encountering the warm saltier Brazil Current at 38.6°S in the mean. At the
157 confluence the flow spreads eastward in a large meander that has its southward latitude at
158 around 45°S . It is interesting to note that this meandering and the circulation in this re-
159 gion is very similar to what is observed from Argo float data at a nominal depth of 1000 m
160 [*Schmid and Garzoli, 2010*] indicating the strong barotropicity of the flow. Also depicted
161 in the surface circulation and in agreement with the circulation at the intermediate water
162 level is the presence of the Zapiola eddy [*de Miranda et al., 1999*] at about 45°S , 45°W .
163 East of the confluence, the Brazil and Malvinas currents flow east southeastward across
164 the South Atlantic, with distinct cores delineating the southern edge of the subtropical
165 gyre from the Antarctic Circumpolar Current system.

4. Variability of the Confluence

166 The confluence latitude is defined from the merged velocity field as the latitude where
167 the surface current vectors interpolated to the 1000 m isobath (which defines the edge of
168 the continental shelf; Fig. 1, top) change direction from southward (Brazil Current) to
169 northward (Malvinas Current) in 77-day (10 frames) lowpassed velocity fields. The time
170 series of the confluence latitude (Fig. 3, top) shows significant annual and interannual
171 variability. A fit with an annual and semiannual cycle (superimposed on Fig. 3) explains
172 13% of the total variance. A monthly climatology was constructed by averaging the value
173 for every month (subpanel, Fig. 3, top). The southernmost extension of the confluence

174 front is observed during austral summer and the northernmost extension during winter,
175 in agreement with previous studies [*Peterson and Stramma, 1991; Garzoli, 1993; Matano*
176 *et al., 1993*]. The maximum and minimum values of the low-passed confluence latitude for
177 each month are also shown in Fig. 3 (sub-panel), showing a maximum northward extension
178 in June 1997 and 2000 (both 35.8°S) and southward extension in March 2005 (40.3°S).
179 This annual range is consistent with *Saraceno et al. [2004]*, who derived the location of
180 the front from Advanced Very High Resolution Radiometer SST for the period 1987–1995,
181 and showed that the front crossed the 1000m isobath between $37\text{--}38.5^{\circ}\text{S}$. The confluence
182 was located north of 37°S in 1993, 1997, 1999 and 2000, but not in the subsequent eight
183 years.

184 Alternatively, the confluence latitude can be defined from sea height along ascending
185 T/P track 163 (Fig. 1), which runs from low values in the Malvinas Current to high values
186 in the Brazil Current. The lowest and highest points are identified in sea height averaged
187 over 77 days (as done with currents), and the confluence latitude is then identified as
188 the latitude where sea height has climbed $3/4$ of the way from the Malvinas minimum to
189 the Brazil maximum. The arbitrary choice of $3/4$ was made so that the mean location
190 of the confluence was the same as in the velocity field definition; smaller choices produce
191 very similar results with a mean shifted to the south. Two examples of identifying the
192 confluence from sea height are shown in Fig. 1 (bottom). The error in sea height is
193 projected onto an error in the confluence latitude by finding the range of latitudes that
194 meet the $3/4$ criterion (dashed lines in Fig. 1, bottom). Larger error bars in the estimated
195 confluence latitude are produced by larger errors in sea height, and also by a weak along-
196 track sea height gradient which spreads the error over a larger latitude range. The resulting

197 time series of confluence latitude (Fig. 3, bottom) is qualitatively similar to the time series
198 calculated from the merged velocity product, with similar peaks and troughs. Errors are
199 largest during the northern extrema in late 1993–early 1994, mid-1994 (which was not a
200 dramatic peak in the velocity-derived time series), mid-1997 and mid-2000, when along-
201 track sea height gradients are reduced.

202 Of particular interest in the time series of confluence latitude is the trend indicating
203 that the confluence front has moved southward over the last 14 years, at a mean rate of
204 -0.86 ± 0.19 degrees per decade in the velocity-based time series (negative is southward),
205 -0.64 ± 0.20 degrees per decade in the sea height (SH)-based time series. A similar trend
206 was identified in an analysis of AVISO altimetry conducted by Gustavo Goni and Pedro
207 DeNezio (G. Goni, pers. comm.). Our standard error estimates are derived from bootstrap
208 resampling of the time series, and include the formal error in confluence latitude for the
209 SH-based estimate. This result can be independently confirmed in the trend of NNR SST
210 anomaly with respect to mean seasonal cycle over the same time period (shading, Fig. 2)
211 which indicates warming of $1.64 \pm 0.25^\circ\text{C}$ in the region $34\text{--}38^\circ\text{S}$, $53.5\text{--}57^\circ\text{W}$ (Fig. 4),
212 centered over the continental shelf on the shallow inshore side of the southward-trending
213 Brazil Current. Much of this southward motion took part early in the time period: the
214 trend in the seasonal-removed confluence latitude for 1 January 1993–31 December 2001
215 was -1.0 ± 0.4 degrees per decade (from velocity), -1.3 ± 0.6 degrees per decade (from SH),
216 while the trend for 1 January 2002–31 December 2007 was $+0.3 \pm 0.5$ (velocity) or $+0.4 \pm 0.8$
217 (SH) degrees per decade (northward, but not significantly different from zero).

218 The confluence location may change because of changes in the transport of the confluent
219 currents or changes in the wind stress pattern [*Matano et al.*, 1993; *Wainer et al.*, 2000].

220 To investigate these possible sources of variability, an analysis is performed both of the
221 surface transports derived from the surface current fields and of the wind field in the
222 area. Upper ocean surface transports can be estimated by assuming that the total surface
223 velocity is uniform in the upper 30 meters and integrating the velocity across the currents.
224 Results (Fig. 5) indicate that at 32°S the surface transport is ~ 2 Sv to the southwest,
225 consistent with the direction of the southward flowing Brazil Current. The direction of
226 the transport starts to change at the confluence (38.6°S) and becomes northeastward after
227 that (~ 2 Sv at 45°S) indicating the presence of the Malvinas Current. The long-term trend
228 observed in the location of the confluence is not apparent in the surface transport values
229 away from the confluence, suggesting that transport changes did not drive the 1993-2007
230 trend, although we must note that our analysis cannot detect subsurface changes not
231 seen in the surface currents. This may be particularly important for the more stratified,
232 baroclinic Brazil Current, which may have significant subsurface transport variability. In
233 addition, these results do not reflect the implicit errors in our velocity product.

234 The relation between the trend in the confluence latitude and the wind stress curl can
235 be examined using fields from the NNR product. SST anomalies (SSTA) were calculated
236 by removing the mean seasonal cycle at each grid point. The spatial distribution of SSTA
237 trend during 1993-2002 (Fig. 2, background shading) reveals that warming occurred
238 across the basin, between 24-40°S. In contrast, during the same period, cooling occurred
239 in the eastern basin between 38-60°S. This distribution of SSTA would produce anomalous
240 atmospheric subsidence at $\sim 50^\circ$ S and convection at $\sim 30^\circ$ S, with consequent surface flow in
241 geostrophic balance creating anomalous easterly winds centered on $\sim 40^\circ$ S. Such a pattern,
242 superimposed on the background time-mean zonal wind stress (maximum Westerlies at

243 50°S; maximum gradient near 40°S; zero at 30°S), would shift the latitude of the maximum
244 curl to the south as it reduces the strength of the northern edge of the Westerlies. The
245 trend in zonal wind stress (Fig. 6, top left) during 1993-2008 has negative (easterly)
246 values in the region 30–45°S, west of about 10°W, indicating weakening of the northern
247 Westerlies and consistent with a southward shift in the maximum wind stress curl. The
248 overall positive trend in zonal wind stress south of 50°S is in agreement with the trend in
249 the Southern Annular Mode, which increased over the time period 1968-2000 [*Limpasuvan*
250 *and Hartmann, 1999; Marshall, 2003*]. In this region, wind energy input calculated as a
251 scalar product of the wind stress increased by over 12% in the past 25 years [*Huang et al.,*
252 *2006*]. Trends in the meridional wind stress (Fig. 6, top right) are weak north of 50°S.
253 As a consequence of these wind stress trends, the wind stress curl (Fig. 6, bottom left)
254 increased across most of the basin at the mean latitude of the confluence, and the basin
255 averaged maximum in the wind stress curl field (Fig. 6, bottom right) shifted southward.

256 The latitude of the maximum in the basin-averaged wind stress curl (Fig. 6, bottom
257 right) follows an annual cycle that, as previously noted by models and observations, is
258 similar to the one followed by the confluence [*Garzoli and Giulivi, 1994*]: shifted to the
259 north in austral winter and to the south in austral summer. A linear fit to the latitude of
260 maximum basin-averaged stress for the period October 1992-December 2007 has a trend
261 of -1.06 ± 0.56 degrees per decade, similar to the trend observed for the confluence front,
262 suggesting that a southward shift in the maximum of the wind stress curl forced the
263 observed trend in the confluence latitude via Sverdrup dynamics, i.e., a western boundary
264 response to latitude of maximum equatorward interior flow [*Wainer et al., 2000*]. If the
265 latitude of the maximum curl is a reliable proxy for the confluence latitude, its earlier

266 history (Fig. 7, top) suggests that the 1993-2007 trend may be part of a longer-term
267 decadal to multidecadal oscillation, which was at an unusually northward location in late
268 1992 through 1993 when the TOPEX/Poseidon altimeter was launched and the AVISO
269 product begins.

5. Discussion and Summary

270 At seasonal time scales, the migration of the confluence front is driven by variations in
271 the wind stress curl field [*Matano et al.*, 1993; *Vivier et al.*, 2001], which in turn are driven
272 by the seasonal cycle of the South Atlantic subtropical basin SST. This can be illustrated
273 by the correlation between the annually highpassed (to remove interannual to decadal fluc-
274 tuations) latitude of basin-averaged curl and other surface properties (Fig. 8, left panels).
275 Superimposed on these seasonal variations, over the 14 years covered by the combined
276 drifter/altimeter observations, the confluence has moved southward at a mean rate of
277 -0.86 ± 0.19 degrees per decade estimated from surface currents, or -0.64 ± 0.20 degrees per
278 decade estimated from sea height along a T/P ground track. Upper 30 m transports of the
279 associated Brazil, Malvinas and North Brazil currents all undergo significant seasonal and
280 interannual variability, but no longer-term trends were observed except in the immediate
281 vicinity of the confluence itself.

282 The time series of the maximum basin-averaged wind stress has a similar trend as the
283 latitude of the confluence, -1.06 ± 0.56 degrees per decade, with most of the southward
284 shift happening early in the period, as seen with the confluence latitude. This strongly
285 suggests that the trend in the confluence location is driven by the shift in the maximum of
286 the wind stress curl at these longer time scales, as it is at the seasonal time scale. Because
287 the curl can be calculated at earlier times than the drifter/altimetry-derived time series,

288 the latitude of the maximum wind stress curl can serve as a proxy for the confluence
289 latitude before October 1992. The earlier part of this proxy record (Fig. 7, top) shows
290 a weak northward trend in the location of the maximum of the curl from 1979 to 1992,
291 suggesting that the observed trend may be part of a decadal to multidecadal oscillation
292 that has been inferred from the northernmost winter location of the confluence front in SST
293 records [*Zavialov et al.*, 1999]. The correlation between the lowpassed (seasonal removed)
294 latitude of maximum basin-averaged curl and various surface properties (Fig. 8, right
295 panels) suggests a similar mechanism to that acting at seasonal time scales: SST variations
296 modifying the wind field, which shifts the confluence latitude via Sverdrup dynamics.
297 However, while seasonal fluctuations of the confluence location are inversely correlated
298 with SST anomalies over the entire subtropical basin, the low frequency variations are
299 inversely correlated with SST anomalies along the Agulhas/Benguela pathway linking the
300 Indian and Atlantic basins. (Correlations along the front in the southwest Atlantic are
301 associated with the SST gradient across the confluence front, and are an independent
302 confirmation of the wind stress curl proxy for confluence location.)

303 It is clear that the confluence is not responding to the generally increasing (in the time
304 period 1968-2000) Southern Annular Mode [*Limpasuvan and Hartmann*, 1999; *Marshall*,
305 2003]. The SST anomaly (SSTA) in the eastern South Atlantic basin (Fig. 7, bottom)
306 has similar low frequency behavior as the wind stress curl maximum (Fig. 7, top) during
307 the period of the observations, with an opposite sign. In both cases a pronounced extreme
308 is found in 1992-1993.

309 The correlation between the confluence location and SST fluctuations (Fig. 8, right)
310 suggests that forcing from the Indian Ocean, via Agulhas leakage, may play a significant

311 role in governing low frequency variations of the confluence location. However, it is
312 interesting, albeit speculative, to note that a local positive feedback could also play a role.
313 As described earlier, warm SST anomalies at the latitude of the confluence will alter the
314 wind pattern such that the maximum curl shifts to the south, driving the confluence front
315 southward. But this in turn could reinforce the SST anomaly field, as subtropical waters
316 penetrate further south. This feedback could continue until the maximum in the wind
317 stress curl reaches 38-40°S. South of that point, the superposition of an easterly anomaly
318 on the mean westerly winds would not alter the latitude of the maximum basin-averaged
319 curl, instead only serving to weaken the Westerlies. It is impossible to separate cause
320 from effect in our correlation map (Fig. 8, bottom right), and the simplest hypothesis
321 to explain the band of high negative correlation in lowpassed SSTA is that it reflects
322 the meridional shifting of the front. However, such a speculative feedback mechanism
323 cannot be ruled out, and could be tested more rigorously in the framework of a coupled
324 ocean/atmosphere model.

325 **Acknowledgments.** The authors were supported by NOAA's Office of Climate Ob-
326 servations and the Atlantic Oceanographic and Meteorological Laboratory. Conversations
327 and input from Martin Visbeck, Gustavo Goni, Ricardo Matano, Edmo Campos and Pe-
328 ter Zavialov were extremely valuable, as were two anonymous reviews. Carmen Alex
329 performed data reduction and supporting computations. Satellite-tracked drifting buoys
330 of the Global Drifter Program are funded as part of NOAA's Global Ocean Observing
331 System.

References

- 332 Blanke, B., M. Arhan, G. Modec, and S. Rocheet (1999), Warm water paths in the
333 equatorial Atlantic as diagnosed with a general circulation model, *J. Phys. Oceanogr.*,
334 *29*, 2453–2768.
- 335 Garzoli, S. L. (1993), Geostrophic velocity and transport variability in the Brazil-Malvinas
336 Confluence, *Deep Sea Res., Part I*, *40*, 1379–1403.
- 337 Garzoli, S. L., and A. Bianchi (1987), Time-space variability of the local dynamics of the
338 Malvinas-Brazil Confluence as revealed by inverted echo sounders, *J. Geophys. Res.*,
339 *92*, 1914–1922.
- 340 Garzoli, S. L., and Z. Garraffo (1989), Transports, frontal motions and eddies at the
341 Brazil-Malvinas currents confluence, *Deep Sea Res.*, *36*(5), 681–703.
- 342 Garzoli, S. L., and C. Giulivi (1994), What forces the variability of the south western
343 Atlantic boundary currents?, *Deep Sea Res.*, *41*(10), 1527–1550.
- 344 Garzoli, S. L., and A. L. Gordon (1996), Origins and variability of the Benguela Current,
345 *J. Geophys. Res.*, *101*, 897–906.
- 346 Garzoli, S. L., A. Gordon, V. Kamenkovich, D. Pillsbury, and C. Duncombe-Rae (1996),
347 Variability and sources of the south eastern Atlantic circulation, *J. Mar. Res.*, *54*,
348 1039–1071.
- 349 Goni, G., and I. Wainer (2001), Investigation of the Brazil Current front dynamics from
350 altimeter data, *J. Geophys. Res.*, *106*(C12), 31,117–31,128.
- 351 Gordon, A. L., and C. L. Greengrove (1986), Geostrophic circulation of the Brazil-
352 Falkland confluence, *Deep Sea Res.*, *33*(5), 573–585.

- 353 Huang, R. X., W. Wang, and L. L. Liu (2006), Decadal variability of wind energy input
354 to the world ocean, *Deep Sea Res., Part II*, 53, 31–41.
- 355 Kalnay, E., et al. (1996), The NCEP/NCAR 40-year reanalysis project, *Bull. Am. Mete-*
356 *orol. Soc.*, 77, 347–471.
- 357 Kushnir, Y., W. A. Robinson, I. Bladé, N. M. J. Hall, S. Peng, and R. Sutton (2002),
358 Atmospheric GCM response to extratropical sst anomalies: Synthesis and evaluation,
359 *J. Climate*, 15, 2233–2256.
- 360 Le Traon, P., F. Nadal, and N. Ducet (1998), An improved mapping method of multi-
361 satellite altimeter data, *J. Atmos. Oceanic Technol.*, 15, 522–534.
- 362 Limpasuvan, V., and D. L. Hartmann (1999), Eddies and the annular modes of climate
363 variability, *Geophys. Res. Letters*, 26, 3133–3136.
- 364 Lumpkin, R., and S. L. Garzoli (2005), Near-surface circulation in the tropical Atlantic
365 Ocean, *Deep Sea Res., Part I*, 52(3), 495–518, 10.1016/j.dsr.2004.09.001.
- 366 Lumpkin, R., and M. Pazos (2007), Measuring surface currents with Surface Velocity Pro-
367 gram drifters: the instrument, its data and some recent results, in *Lagrangian Analysis*
368 *and Prediction of Coastal and Ocean Dynamics*, edited by A. Griffa, A. D. Kirwan,
369 A. Mariano, T. Özgökmen, and T. Rossby, chap. 2, pp. 39–67, Cambridge University
370 Press.
- 371 Marshall, G. J. (2003), Trends in the Southern Annular Mode from observations and
372 reanalyses, *J. Climate*, 16, 4134–4143.
- 373 Matano, R. P., M. G. Schlax, and D. B. Chelton (1993), Seasonal variability in the South
374 Atlantic, *J. Geophys. Res.*, 98(C10), 18,027–18,035.

- 375 de Miranda, A. P., B. Barnier, and W. K. Dewar (1999), On the dynamics of the Zapiola
376 Anticyclone, *J. Geophys. Res.*, *104*(C9), 21,137–21,149.
- 377 Niiler, P. P. (2001), The world ocean surface circulation, in *Ocean Circulation and Climate*,
378 *International Geophysics Series*, vol. 77, edited by G. Siedler, J. Church, and J. Gould,
379 pp. 193–204, Academic Press.
- 380 Niiler, P. P., N. A. Maximenko, G. G. Panteleev, T. Yamagata, and D. B. Olson (2003),
381 Near-surface dynamical structure of the Kuroshio Extension, *J. Geophys. Res.*, *108*(C6),
382 3193, doi:10.1029/2002JC001,461.
- 383 Olson, D., G. P. Podesta, R. H. Evans, and O. B. Brown (1988), Temporal variations in the
384 separation of Brazil and Malvinas currents, *Deep Sea Res., Part A*, *35*(12), 1971–1990.
- 385 Peterson, R. G., and L. Stramma (1991), Upper-level circulation in the South Atlantic
386 Ocean, *Progress in Oceanography*, *26*, 1–73.
- 387 Ralph, E. A., and P. P. Niiler (1999), Wind-driven currents in the Tropical Pacific, *J.*
388 *Phys. Oceanogr.*, *29*, 2121–2129.
- 389 Reynolds, R. W., N. A. Rayner, T. M. Smith, D. C. Stokes, and W. Wang (2002), An
390 improved in situ and satellite SST analysis for climate, *J. Climate*, *15*(13), 1609–1625.
- 391 Richardson, P. L., and S. L. Garzoli (2003), Characteristics of intermediate water flow in
392 the Benguela current as measured with RAFOS floats, *Deep Sea Res., Part II*, *50*(1),
393 87–118.
- 394 Rio, M.-H., P. Schaeffer, G. Moreaux, J.-M. Lemoine, and E. Bronner (2009), A new mean
395 dynamic topography computed over the global ocean from GRACE data, altimetry
396 and in-situ measurements, in *OceanObs09 Symposium, 21-25 September 2009*, poster,
397 Venice, Italy.

- 398 Saraceno, M., C. Provost, A. Piola, J. Bava, and A. Gagliardini (2004), Brazil Malvinas
399 frontal system as seen from 9 years of advanced very high resolution radiometer data,
400 *J. Geophys. Res.*, *109*, C05,027, doi:10.1029/2003JC002,127.
- 401 Schmid, C., and S. L. Garzoli (2010), New observations of the spreading and variability
402 of the Antarctic Intermediate Water in the Atlantic, *J. Mar. Res.*, *67*(6), 815–843.
- 403 Signorini, S. R. (1978), On the circulation and the volume transport of the Brazil Current
404 between the Cape of São Tomé and Guanabara Bay, *Deep Sea Res.*, *25*(5), 481–490.
- 405 Speich, S., B. Blanke, and W. Cai (2007), Atlantic meridional overturning
406 and the southern hemisphere supergyre, *Geophys. Res. Letters*, *34*, L23,614,
407 doi:10.1029/2007GL031,583.
- 408 Stommel, H. (1958), *The Gulf Stream: A Physical and Dynamical Description.*, 202 pp.,
409 Univ. of California Press and Cambridge Univ. Press, Berkeley, CA USA and London,
410 UK.
- 411 Stramma, L., and M. England (1999), On the water masses and mean circulation of the
412 South Atlantic Ocean, *J. Geophys. Res.*, *104*, 20,863–20,883.
- 413 Thompson, D. W. J., and S. Solomon (2002), Interpretation of recent Southern Hemi-
414 sphere climate change, *Science*, *296*, 895–899.
- 415 Vivier, F., C. Provost, and M. P. Meredith (2001), Remote and local forcing in the Brazil-
416 Malvinas region, *J. Phys. Oceanogr.*, *31*(4), 892–913.
- 417 Wainer, I., P. Gent, and G. Goni (2000), Annual cycle of the Brazil-Malvinas conflu-
418 ence region in the National Center for Atmospheric Research climate system model, *J.*
419 *Geophys. Res.*, *105*(C11), 26,167–26,177.

420 Witter, D., and A. Gordon (1999), Interannual variability of South Atlantic circulation
421 from 4 years of TOPEX/POSEIDON satellite altimeter observations, *J. Geophys. Res.*,
422 *104*(C9), 1389–1410.

423 Zavalov, P. O., I. Wainer, and J. M. Absy (1999), Sea surface temperature variability
424 off southern Brazil and Uruguay as revealed from historical data since 1854, *J. Geo-*
425 *phys. Res.*, *104*(C9), 21,021–21,032.

Figure 1. (Top) TOPEX/Poseidon ground track 163 superimposed on 1000m isobaths (shading). (Bottom) total sea height along the ground track (solid line with shaded error bars) on 25 August 1997 (left) and 1 January 2007 (right). Circles indicates the confluence latitude, and heavy dashed lines indicate the error in confluence latitude associated with error in sea height.

Figure 2. Mean surface geostrophic circulation of the South Atlantic derived from a synthesis of surface drifter trajectories, NCEP winds and AVISO sea level anomalies. Shading is sea surface temperature anomaly trend during January 1993- December 2002 ($^{\circ}\text{C}/\text{decade}$) from NCEP/NCAR.v2 reanalysis [*Reynolds et al.*, 2002], with nonzero values shown only where the trend significantly exceeds zero. Warming at the Brazil/Malvinas confluence is consistent with a southward shift of the confluence front.

Figure 3. (Top) confluence latitude (black), with linear trend (dashed) and best-fit annual+semiannual (grey) calculated from the merged velocity field product. The inset shows the monthly climatology, with standard deviation shaded and dashed lines indicating maximum and minimum values observed in each month. (Bottom) confluence latitude determined from sea height along T/P ground track 163, with formal error estimate (shading), linear trend (dashed) and best-fit annual+semiannual (grey).

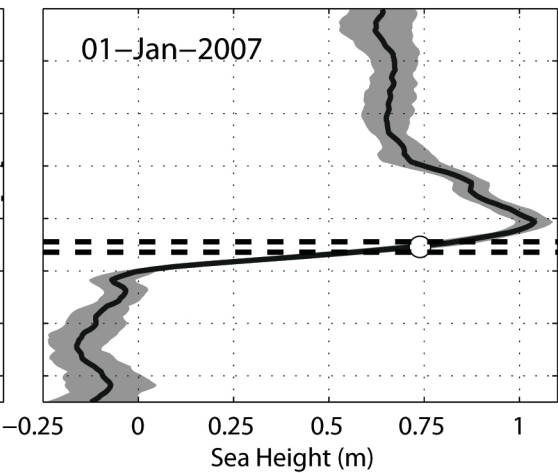
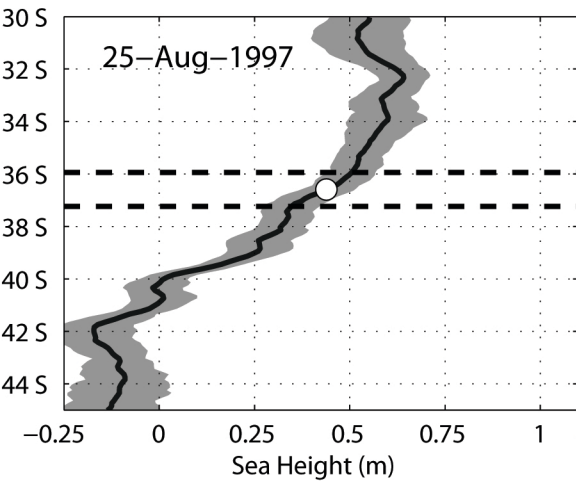
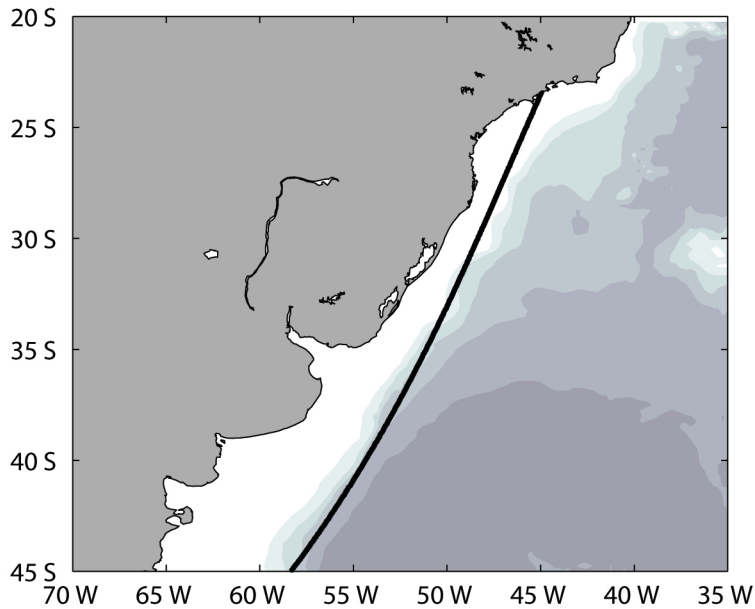
Figure 4. NCEP/NCAR v.2 Reanalysis SST anomaly ($^{\circ}\text{C}$) with respect to time-mean seasonal cycle in the region $34\text{--}38^{\circ}\text{S}$, $53.5\text{--}57^{\circ}\text{W}$. Dashed line indicates the best-fit trend during the period 1993–2002.

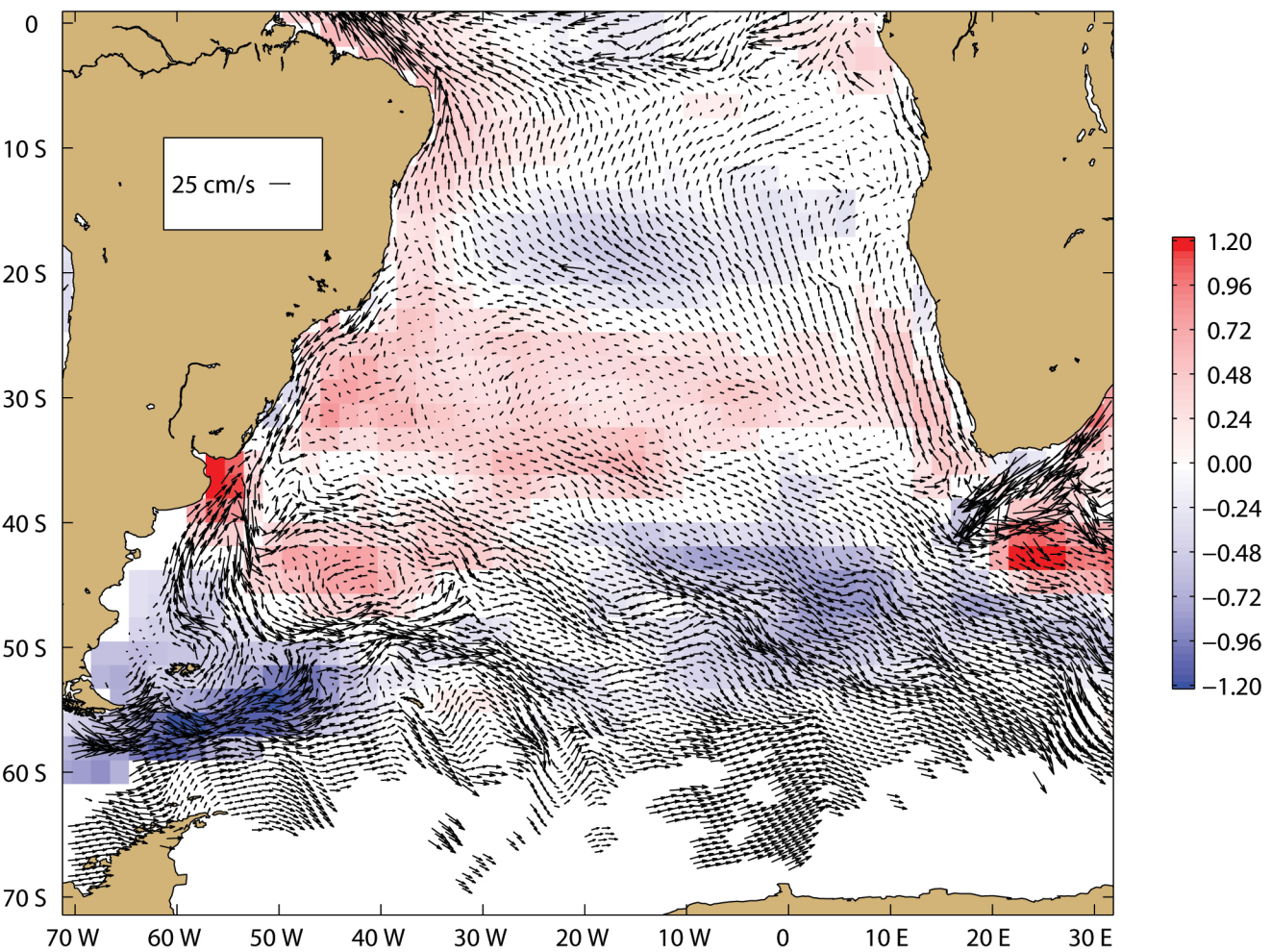
Figure 5. Upper 30 m transport (positive northward) time series of the Brazil Current at 32°S (top) and 34°S (middle, upper), at the mean location of the confluence, 38.6°S (middle, lower), and in the Malvinas Current at 45°S (bottom), calculated from near-surface currents.

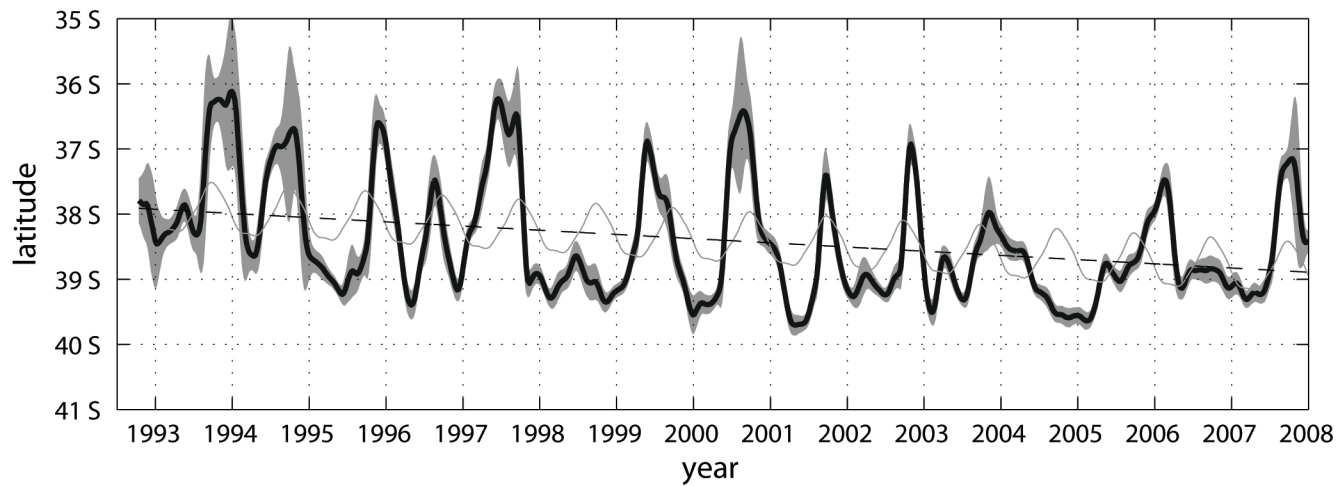
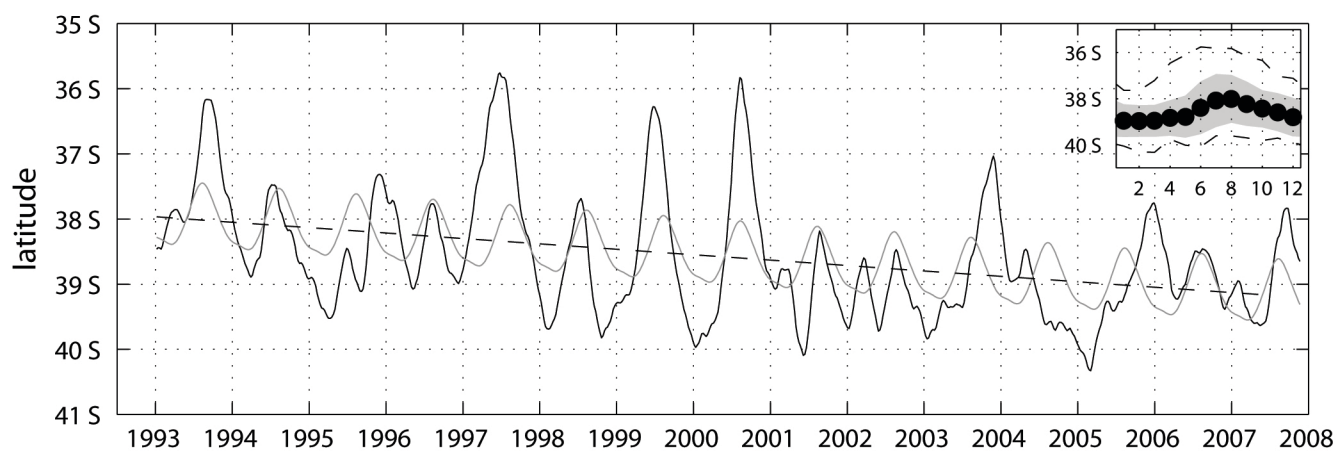
Figure 6. Trend in the zonal and meridional components of the wind stress (top panels) and of the curl of the wind stress (lower left panel) in the decade 1993–2002. Trends are not shown where they are not significantly different from zero. The bottom right panel shows time series of the maximum of the curl of the wind stress across the basin as a function of time. White solid curve is the annual+semiannual fit, black dots are the maxima and the straight line is the slope.

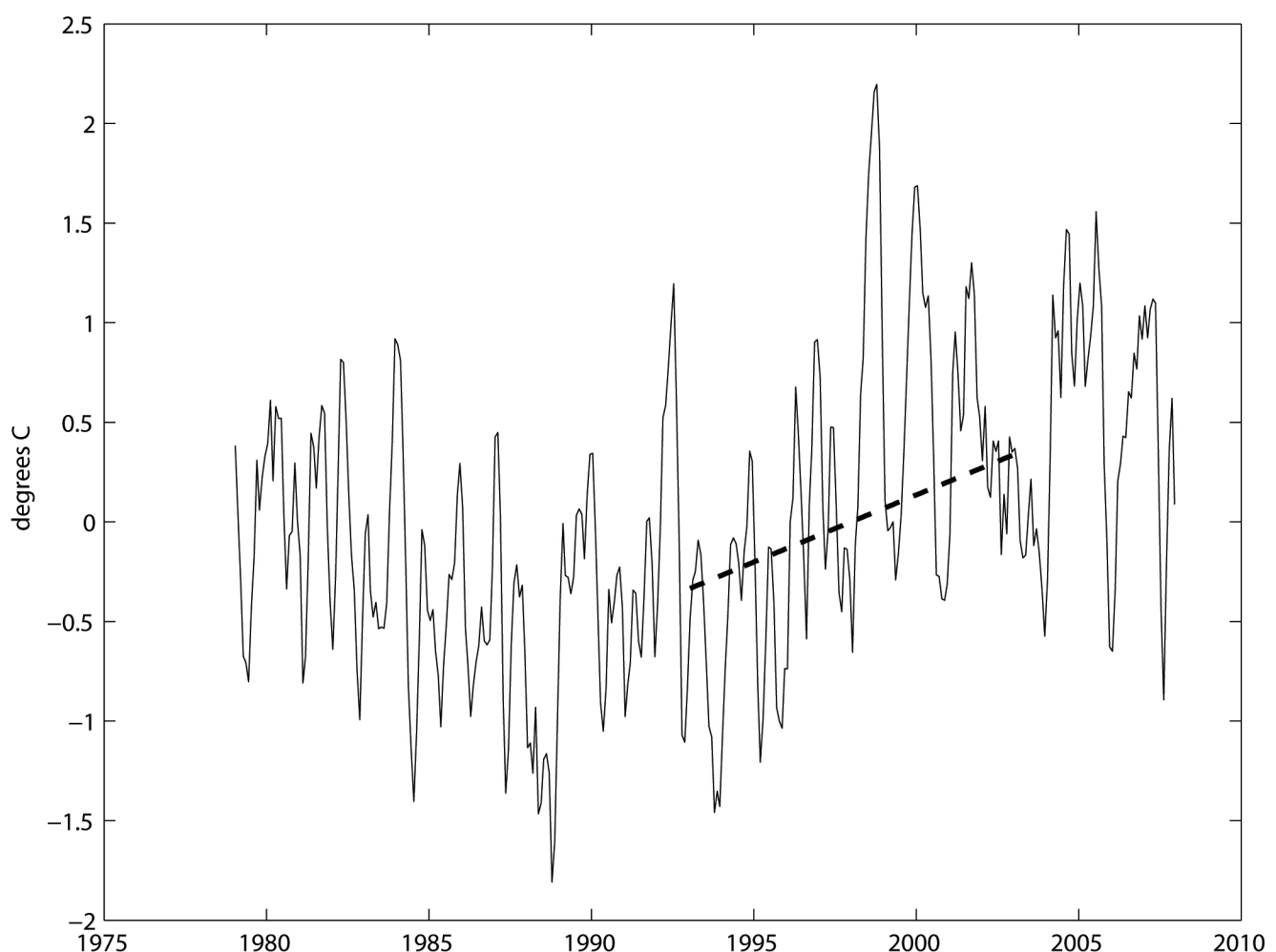
Figure 7. (Top) Time series of the latitude of maximum wind stress curl averaged over the South Atlantic basin, 1979 to present, from NCEP/NCAR reanalysis v2. The thin line is monthly values; heavy black curve is a 365 day lowpass. (Bottom): Time series of sea surface temperature anomaly SST anomaly in the South Atlantic basin, calculated from NCEP/NCAR v.2 reanalysis by removing the monthly climatological mean signal at each grid point, then averaging across the basin in the latitude band 20-40°S.

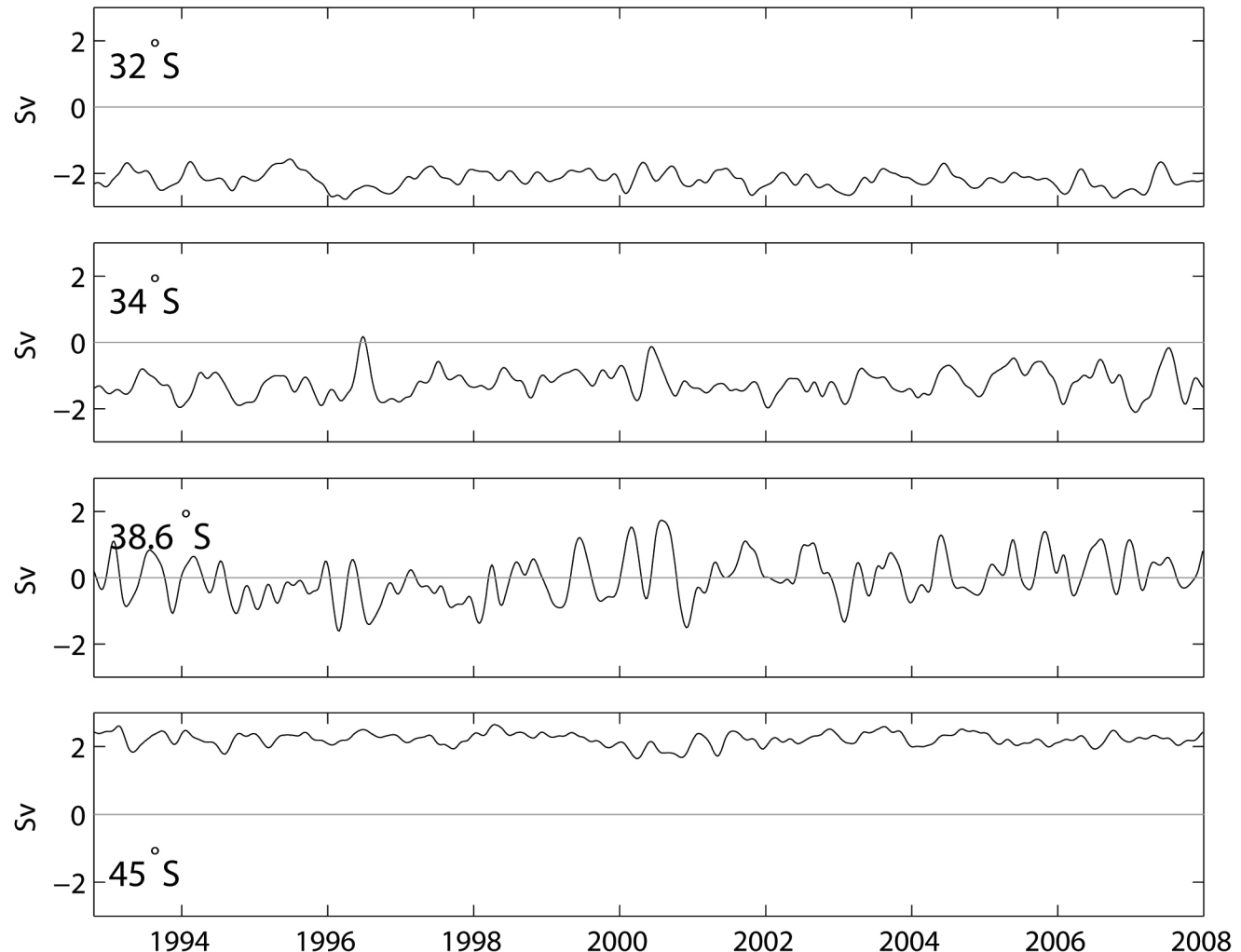
Figure 8. (Top) latitude of the basin-averaged maximum wind stress curl, highpassed (left) and lowpassed (right) at 365 days. Panels below show the zero lag correlation coefficient between this signal and the highpassed (left)/lowpassed (right) zonal wind stress, surface air pressure, and SST.

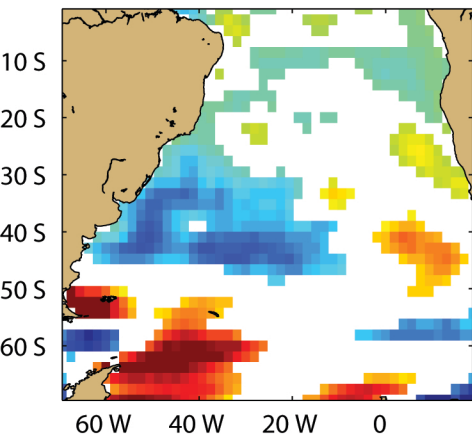
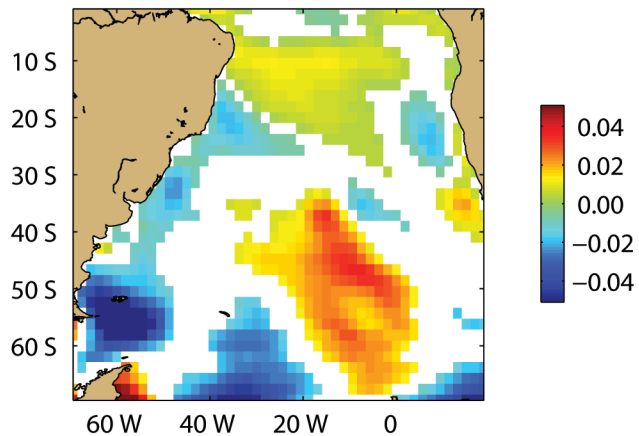
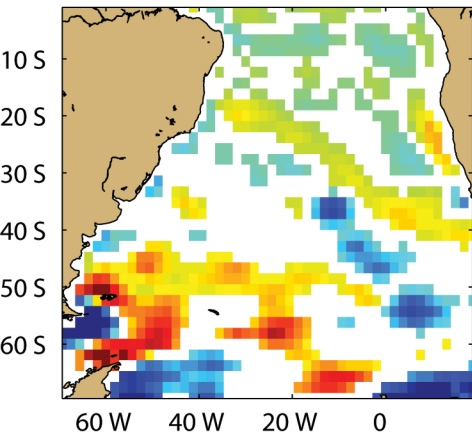
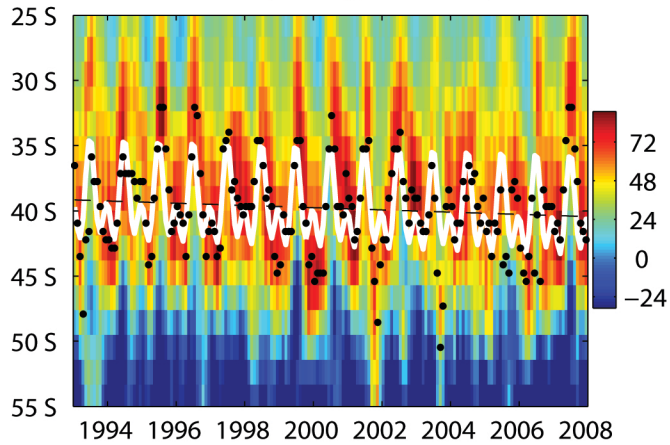


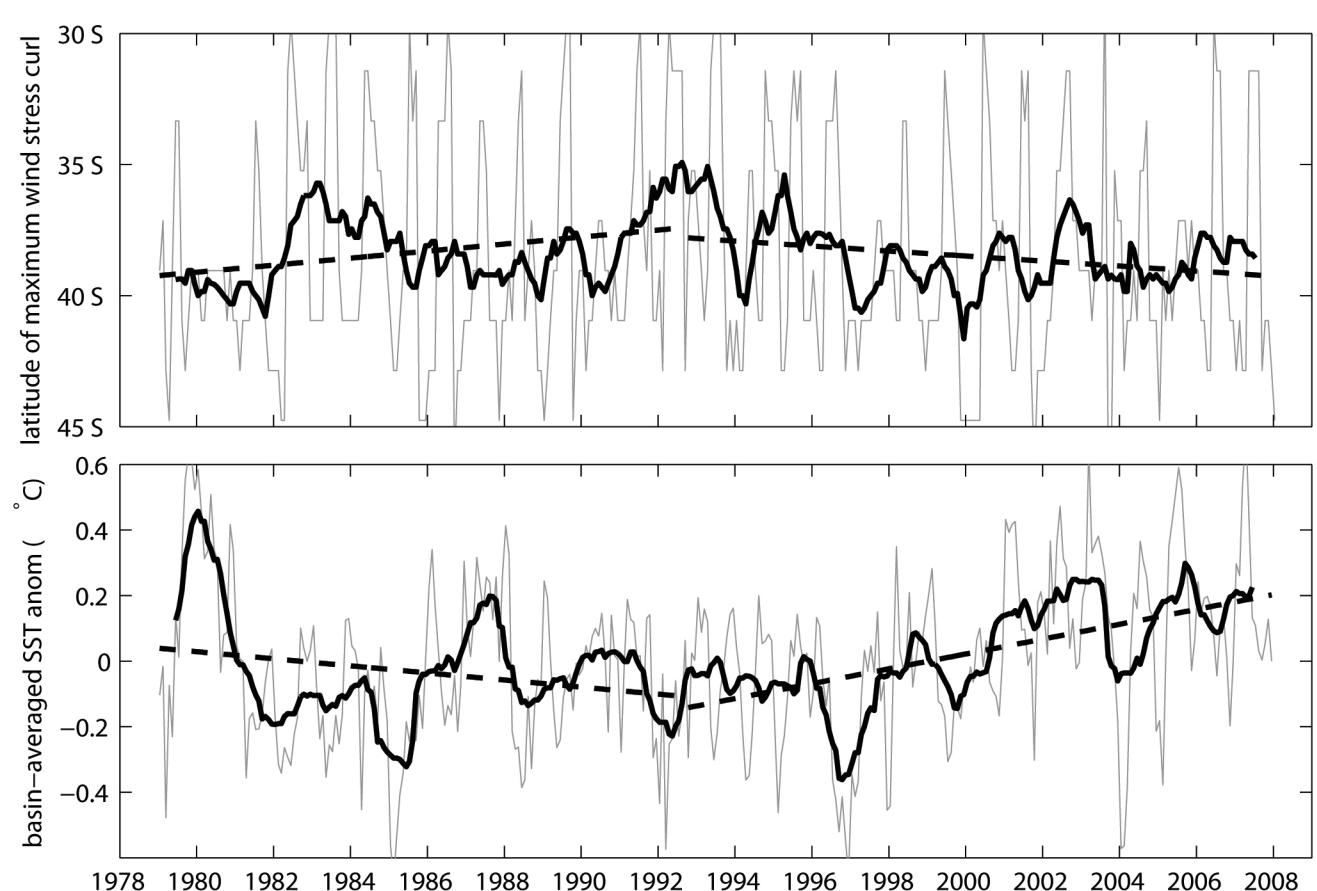




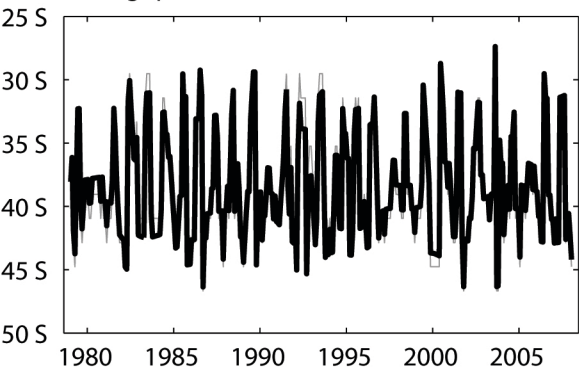




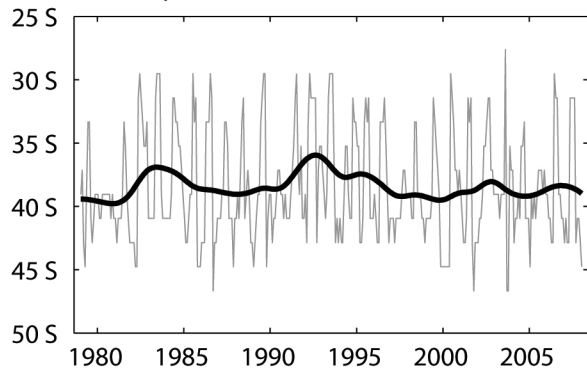
Trend in t_x (Pa/decade)Trend in t_y (Pa/decade)Trend in $\tilde{N}'t$ (Pa/decade)zonal mean $\tilde{N}'t$ (shading, 10^9 Pa/m) and max



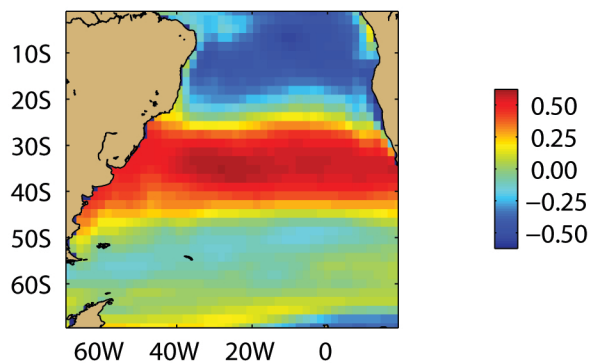
Highpassed latitude of maximum curl



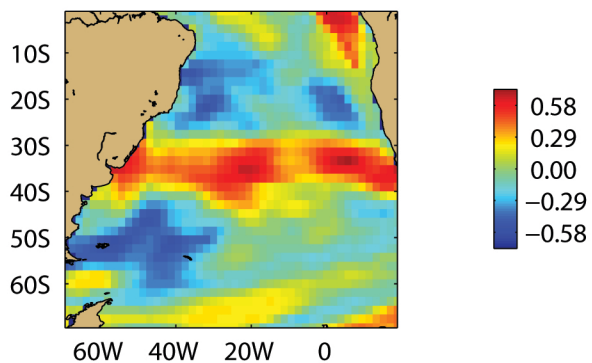
Lowpassed latitude of maximum curl



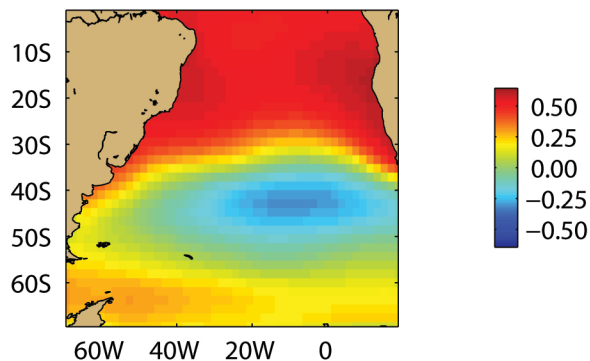
Correlation with zonal wind stress



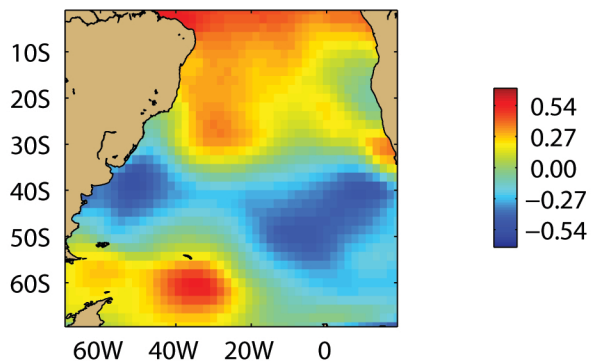
Correlation with zonal wind stress



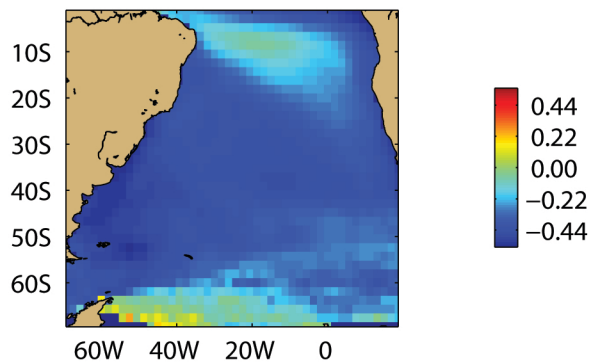
Correlation with surface pressure



Correlation with surface pressure



Correlation with SST



Correlation with SST

